

THE ORIGIN OF HIGH-ENERGY EMISSION IN THE YOUNG RADIO SOURCE PKS 1718–649

MALGOSIA SOBOLEWSKA¹, GIULIA MIGLIORI², LUISA OSTORERO^{3,4}, ANETA SIEMIGINOWSKA¹, ŁUKASZ STAWARZ⁵, MATTEO GUAINAZZI⁶, MARTIN J. HARDCASTLE⁷

¹ Center for Astrophysics | Harvard & Smithsonian, 60 Garden Street, Cambridge, MA 02138, USA.

² INAF, Istituto di Radio Astronomia di Bologna, Via P. Gobetti 101, I-40129 Bologna, Italy

³ Dipartimento di Fisica, Università di Torino, Via P. Giuria 1, 10125 Torino, Italy

⁴ Istituto Nazionale di Fisica Nucleare (INFN), Sezione di Torino, Via P. Giuria 1, 10125 Torino, Italy

⁵ Astronomical Observatory, Jagiellonian University, ul. Orla 171, 30-244 Kraków, Poland

⁶ European Space Research and Technology Centre (ESA/ESTEC), Keplerlaan 1, 2201 AZ, Noordwijk, The Netherlands and

⁷ Department of Physics, Astronomy and Mathematics, University of Hertfordshire, College Lane, Hatfield AL10 9AB, UK

Draft version November 5, 2021

ABSTRACT

We present a model for the broadband radio-to- γ -ray spectral energy distribution of the compact radio source, PKS 1718–649. Because of its young age (100 years) and proximity ($z = 0.014$), PKS 1718–649 offers a unique opportunity to study nuclear conditions and the jet/host galaxy feedback process at the time of an initial radio jet expansion. PKS 1718–649 is one of a handful of young radio jets with γ -ray emission confirmed with the *Fermi*/LAT detector. We show that this γ -ray emission can be successfully explained by Inverse Compton scattering of the ultraviolet photons, presumably from an accretion flow, off non-thermal electrons in the expanding radio lobes. The origin of the X-ray emission in PKS 1718–649 is more elusive. While Inverse Compton scattering of the infrared photons emitted by a cold gas in the vicinity of the expanding radio lobes contributes significantly to the X-ray band, the data require that an additional X-ray emission mechanism is at work, e.g. a weak X-ray corona or a radiatively inefficient accretion flow, expected from a LINER type nucleus such as that of PKS 1718–649. We find that the jet in PKS 1718–649 has low power, $L_j \simeq 2.2 \times 10^{42}$ erg s⁻¹, and expands in an environment with density $n_0 \simeq 20$ cm⁻³. The inferred mass accretion rate and gas mass reservoir within 50-100 pc are consistent with estimates from the literature obtained by tracing molecular gas in the innermost region of the host galaxy with SINFONI and ALMA.

Subject headings: galaxies: active — galaxies: jets — X-rays: galaxies — radiation mechanisms: nonthermal

1. INTRODUCTION

PKS 1718–649 is a well known radio source in NGC 6328 classified as a low-ionization nuclear emission-line region (LINER) galaxy with photoionization as the main excitation mechanism of emission lines (Filippenko 1985). It hosts a supermassive black hole with a mass of the order of $10^8 M_\odot$ (Willett et al. 2010). The radio source has convex radio spectrum peaking in the GHz range (Tingay et al. 2015) and it belongs to the class of Gigahertz-Peaked Spectrum sources (GPS; e.g. O’Dea 1998; O’Dea & Siemiginowska 2016; O’Dea & Saikia 2021). GPS sources with radio lobes that show symmetric morphology, as in the case of PKS 1718–649 (Tingay et al. 1997), are known as Compact Symmetric Objects (CSOs; e.g. O’Dea & Saikia 2021; Orienti 2016; Wilkinson et al. 1994). They appear to be smaller versions of classical doubles (i.e., Fanaroff-Riley type II radio galaxies; Fanaroff & Riley 1974). Multi-epoch radio monitoring of the expansion of the lobes of PKS 1718–649 implies that the radio source is very young, $t_{\text{age}} \simeq 100$ years, and small, with parsec scale linear radio size (Polatidis & Conway 2003; Angioni et al. 2019). At its redshift of $z = 0.0144$ (Meyer et al. 2004), it is the nearest known CSO with a measured kinematic age known to date (An & Baan 2012).

PKS 1718–649 is currently one of the best studied ex-

amples of a newly-born radio source, observed and detected across the whole electromagnetic spectrum, from the radio to the γ -ray band. The source has been observed spectroscopically in the mid infra-red band (MIR) with *Spitzer* and showed signatures typical of both star-forming gas and active galactic nucleus (AGN) gas illumination (Willett et al. 2010). Filippenko (1985) demonstrated that the optical light of the host galaxy of PKS 1718–649 contains a contribution from a non-stellar power-law continuum that might be associated with weak nuclear emission. Siemiginowska et al. (2016) observed PKS 1718–649 with *Chandra* for the first time in the X-ray band and found that a point source is embedded in extended X-ray emission that was studied in detail by Beuchert et al. (2018). The detection of PKS 1718–649 in the γ -ray band was first reported by Migliori et al. (2016) and then confirmed by the Fermi-LAT 4th Source catalog (Abdollahi et al. 2020). In general, symmetric radio sources are not expected to be strong γ -ray emitters, as opposed to blazars in which the emission is enhanced due to the jet orientation. However, Stawarz et al. (2008) and Ostorero et al. (2010) posited that CSO high-energy emission, in particular γ -ray emission, is expected due to Inverse Compton (IC) scattering of the ambient low-energy photons off the non-thermal electron populations within the expanding radio lobes inflated by the radio jet. While CSOs are indeed regularly detected in the X-ray band even in short exposures (e.g. Siemigi-

nowska et al. 2009; Sobolewska et al. 2019a; and references therein), PKS 1718–649 remains one of only a handful of γ -ray emitters with a firm CSO classification to date (Principe et al. 2020; Lister et al. 2020; Müller et al. 2016)¹.

In this paper, we study the broadband radio-to- γ -ray emission of PKS 1718–649, and identify the physical processes that dominate the high-energy radiative output of a radio source in formation. We first collect the multiwavelength observations of the source to construct its broadband spectral energy distribution (SED; Section 2). We then model the observed SED in the framework of the expanding radio lobe model of Stawarz et al. (2008; Section 3). We present our results in Section 4, we discuss our findings in Section 5, and conclude in Section 6. Throughout the paper, we use the most recent constraints on the cosmological parameters to convert the observed fluxes into luminosities (Hinshaw et al. 2013; $H_0 = 69.3 \text{ km s}^{-1} \text{ Mpc}^{-1}$, $\Omega_m = 0.287$, implemented as WMAP9 in the `astropy.cosmology` package (Astropy Collaboration 2013; 2018).

2. MULTIWAVELENGTH DATA OF PKS 1718–649

In this section, we summarize the multiwavelength observations of PKS 1718–649. We show the observed SED of the source in Figure 1. We use the observational constraints in Section 4 to differentiate among various models of the broadband SED for PKS 1718–649.

2.1. Radio and submillimeter

PKS 1718–649 has been thoroughly studied in the radio band with the Parkes telescope (Bolton & Butler 1975; Gregory et al. 1994), Very Large Array (VLA; Healey et al. 2007), Australia Telescope Compact Array (ATCA; Wright & Otrupcek 1990; Verón-Cetty et al. 1995; Tingay et al. 1997, 2015; Tingay & de Kool 2003; Ricci et al. 2006; Sadler et al. 2006; Massardi et al. 2008; Murphy et al. 2010; Maccagni et al. 2014), Murchison Widefield Array (MWA; Tingay et al. 2015). The source has been detected with the Wilkinson Microwave Anisotropy Probe (WMAP; Bennett et al. 2003; Chen & Wright 2009; Giommi et al. 2009; Massardi et al. 2009; Wright et al. 2009; Gold et al. 2011) and a continuum flux measurement of 0.304 Jy at 230 GHz has been obtained with the Atacama Large Millimeter/submillimeter Array (ALMA, Maccagni et al. 2018). Representative radio to submillimeter flux measurements are collected in Figure 1.

The Very-Long-Baseline Interferometry (VLBI) observations at 4.8 GHz revealed a compact double-sided structure with linear size $LS \sim 2 \text{ pc}$ (Tingay et al. 1997, 2002; Angioni et al. 2019) and no apparent radio emission from the core (Tingay et al. 2002). Multi-epoch radio monitoring allowed the derivation of the hot spot advance velocity, $v_h = 0.07c$ (Giroletti & Polatidis 2006), which implied that the kinematic age of the radio source in PKS 1718–649 is ~ 100 years (see also Angioni et al. 2019). Recent observations of PKS 1718–649 with ATCA and MWA allowed Tingay et al. (2015) to conclude that the radio data of the source are best modeled

with an inhomogeneous free-free absorption model (Bicknell et al. 1997). We plot the best fitting models derived by Tingay et al. (2015) for their three observing runs in Figure 1.

2.2. Infrared and optical/ultraviolet

The source has been detected in the mid-infrared (MIR) band with the Wide-field Infrared Survey Explorer (WISE); we include in Figure 1 the 4-band fluxes from the AllWISE source catalog published by Cutri et al. (2013). Willett et al. (2010) reported on *Spitzer* observations of PKS 1718–649. A 5.2–38 μm MIR spectrum of the source has been obtained, and peakup fluxes of $F(16\mu\text{m}) = 49 \text{ mJy}$ and $F(22\mu\text{m}) = 57 \text{ mJy}$ have been measured with 15% measurement error (see Figure 1).

In addition, the authors detected a spectrally resolved [OIV] 25.8 μm line, which allowed them to estimate the mass of the black hole in PKS 1718–649, using the relation by Dasyra et al. (2008), $\log(M/M_\odot) = 8.62 \pm 0.45$, consistent with the mass they derived using the $L_{\text{bulge}}-M_{\text{BH}}$ relation of Bentz et al. (2009), $\log(M_{\text{BH}}^{\text{bulge}}/M_\odot) = 8.48$. The MIR view of PKS 1718–649 revealed a moderately dusty environment and a low star-formation rate in the host galaxy. The authors argue that a recent merger triggered the AGN activity, but also stripped the star-forming gas from the galaxy.

Veron-Cetty et al. (1995) argued that the host of PKS 1718–649 resembles a high luminosity elliptical galaxy with a faint outer spiral structure, which most likely originated in a merger involving a gas-rich spiral in the process of forming an elliptical. Optical spectroscopy of PKS 1718–649’s host galaxy, NGC 6328, was presented in Filippenko (1985). The subtraction of an elliptical galaxy template revealed a weak non-stellar power-law component classified as a LINER AGN, which was found to contribute approximately half the strength of starlight near 3200 Å.

2.3. High energies

PKS 1718–649 was observed for the first time in X-rays with *Chandra* in 2011 for 5 ks as part of our CSO X-ray survey (Siemiginowska et al. 2016). This initial observation revealed that the X-ray spectrum of the point source can be described by an absorbed power-law model with $\Gamma = 1.6 \pm 0.2$ and $N_H(z) = (0.8 \pm 0.7) \times 10^{21} \text{ cm}^{-2}$, and that it is embedded in diffuse X-ray emission. PKS 1718–649 was then re-observed with *Chandra* in 2014 for a total time of 50 ks and with *XMM-Newton* in 2017 for 20 ks. A simultaneous fit to these multi-epoch data allowed Beuchert et al. (2018) to detect a presence of non-variable emissions due to photoionized and collisionally ionized plasmas; the former was explained as due to nuclear irradiation and the latter as due to supernovae activity in the host galaxy. They constrained the intrinsic photon index to $\Gamma = 1.78_{-0.09}^{+0.10}$, and found variability on the timescale of years in the normalization of the power law emission by a factor of up to ~ 2.5 , and in intrinsic equivalent hydrogen column density in the $(3 - 7) \times 10^{21} \text{ cm}^{-2}$ range. Sobolewska et al. (2019a) showed that, despite its modest intrinsic N_H , PKS 1718–649 is located near the heavily absorbed CSOs (with N_H exceeding 10^{23} cm^{-2}) in the radio size vs. radio luminosity vs. N_H diagram. This makes it a par-

¹ We note that that PMN J1603-4904 studied by Müller et al. (2016) is not included anymore in the latest *Fermi*/LAT catalog.

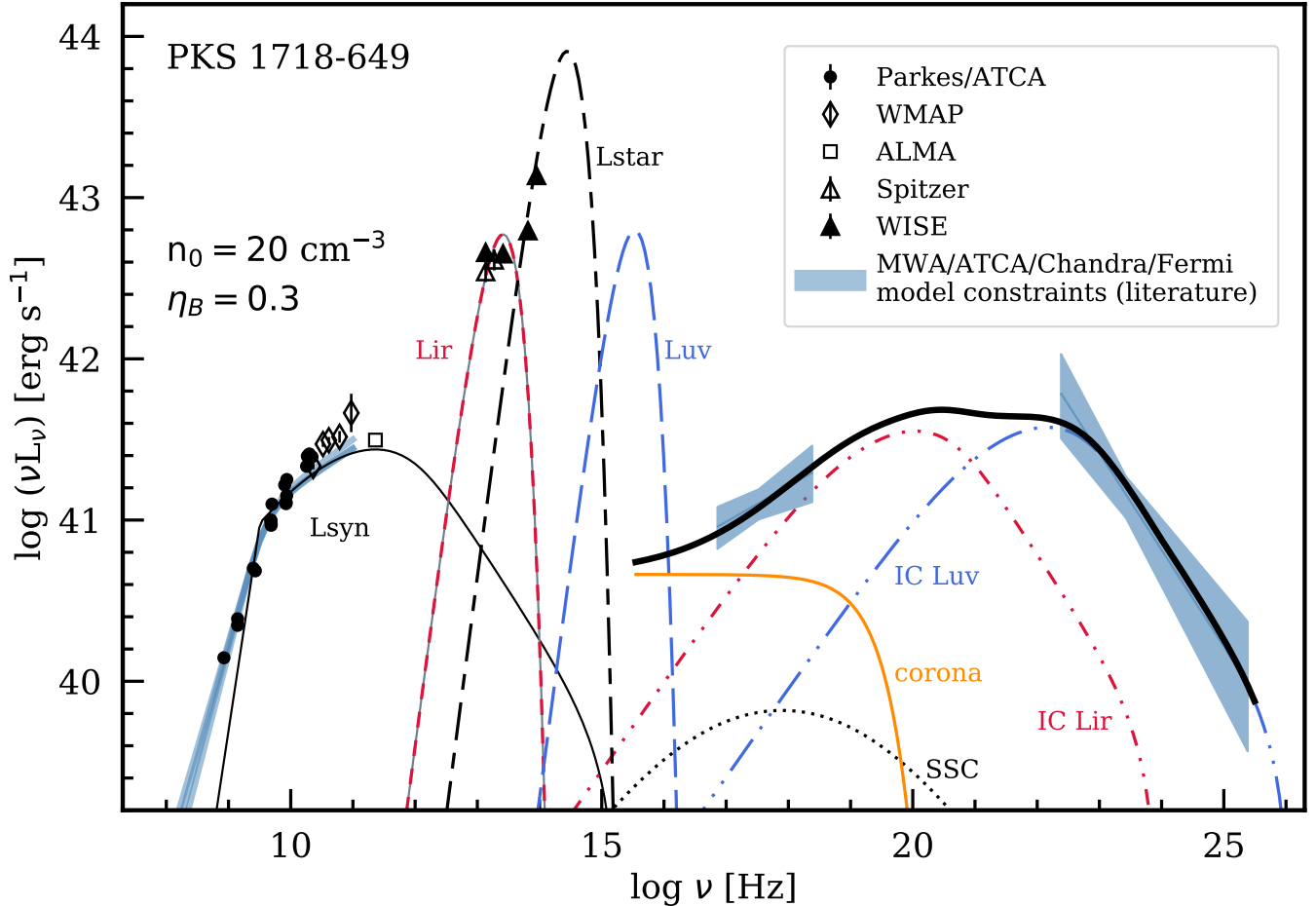


FIG. 1.— Observed broadband spectral energy distribution of PKS 1718–649 and the best-fit theoretical model. Circles – radio data from Mauch et al. (2003), Maccagni et al. (2014), Tingay et al. (2003), Bolton et al. (1975), Massardi et al. (2008), Gregory et al. (1994), Murphy et al. (2010), Wright & Otrupcek (1990), Healey et al. (2007), Ojha et al. (2010), Sadler et al. (2006), Ricci et al. (2006). Diamonds – 9-year WMAP catalog data from Gold et al. (2011). Square – ALMA measurement from Maccagni et al. (2018). Open triangles – Spitzer measurements from Willett et al. (2010). Filled triangles – WISE measurements from Cutri et al. (2013; flux within $8''$). Shaded regions – MWA/ATCA radio model constraints (Tingay et al. 2015); *Chandra* and *XMM-Newton* model constraints on the intrinsic unabsorbed power-law emission (Beuchert et al. 2018); *Fermi*/LAT 1σ model constraints (Principe et al. 2021). Broadband model components are as follows: self-absorbed synchrotron radiation (thin black solid line), three black-body components representing the infrared (short-dashed), starlight (long-short-dashed) and accretion disk photon fields (long-dashed), and their corresponding IC components originating from a single radio lobe. The short-dashed line represents the f_{IR} corresponding to the black body component normalized to L_{IR} at the ν_{IR} frequency. The solid orange (gray in b&w version) line illustrates the contribution of a low-luminosity X-ray nuclear emission (a weak X-ray corona or an ADAF-type emission). The thick black line represent the sum of the IC components and the additional X-ray emission. Model parameters are listed in Table 1.

ticularly interesting target for understanding the impact of the environment on the initial radio source evolution.

PKS 1718–649 was the first CSO detected in the γ -ray band (Migliori et al. 2016). The reported *Fermi*/LAT test statistic was $TS = 36$ ($\sigma \gtrsim 5$) band and $TS = 18.5$ ($\sigma = 4.3$) in the 0.1–100 GeV and 0.2–100 GeV band, respectively. The source has been included in the 4th *Fermi*/LAT catalog (Abdollahi et al. 2020), and its γ -ray properties were revised by Principe et al. (2020), who found the 0.1–100 GeV γ -ray flux and slope of $F_{\text{LAT}} = (5.3 \pm 1.5) \times 10^{-9}$ ph cm $^{-2}$ s $^{-1}$ and $\Gamma_{\text{LAT}} = 2.6 \pm 0.14$, respectively. No significant year-to-year or shorter γ -ray variability was detected from the source.

The confidence regions representing the intrinsic X-ray and γ -ray power law emissions of the source are shown in Figure 1. We adopted the γ -ray power-law parameters as in Principe et al. (2021). In the X-ray band we use the photon index and its error, and a mean X-ray power-

law normalization and its mean error estimated based on the X-ray fits presented in Beuchert et al. (2018). This means that we model only the intrinsic power-law X-ray component arising near the nucleus, and not the extended X-ray emission.

3. BROADBAND MODEL

In order to investigate the origin of high-energy (X/ γ -ray) emission from PKS 1718–649, we model its broadband SED with the dynamical model of Stawarz et al. (2008), where a set of equations originally considered by Begelman & Cioffi (1989) to describe classical doubles expanding in an ambient medium is employed to characterize the evolution of compact sources. In the framework of this model, a relativistic jet with kinetic power L_j propagates in the innermost parts of the host galaxy with a constant velocity, v_h , into a uniform gaseous medium of constant density $\rho = m_p n_0$. The momentum flux of the relativistic jet is balanced by the ram pressure

of the ambient medium spread over some constant area A_h , $L_j/c = m_p n_0 v_h^2 A_h$. Ultra-relativistic electrons with an initial energy distribution $Q(\gamma)$ and Lorentz factors $\gamma_{\min} < \gamma < \gamma_{\max}$ are injected from the terminal hot spots of the jet into the expanding lobes. The electron population of the lobes undergoes adiabatic and radiative cooling in the course of the source growth from an initial size $r_0 = (A_h \pi^{-1} l_c^{-2}) LS$ to LS . Transverse expansion of the source is governed by a scaling law $l_c(t) \propto t^{1/2}$ reproducing the initial, ballistic phase of the jet propagation (e.g. Kawakatu & Kino 2006). The lobe’s electrons inverse-Compton scatter all the ambient low-energy photon populations, which include synchrotron photons, infrared (torus) photons, galaxy starlight, and the ultraviolet radiation of an accretion flow. We approximate the infrared, optical and UV spectra as blackbody components for the purpose of evaluating the IC radiation of the lobes. The synchrotron radiation is described with a synchrotron self-absorbed model. We refer the readers to Stawarz et al. (2008) and Ostorero et al. (2010) for further details of the model.

The model has many parameters. However, high quality observations of PKS 1718–649 across the electromagnetic spectrum allowed us to put constraints on the majority of them (Table 1). We use the linear size of the radio source, $LS = 2$ pc, and the hotspot separation velocity, $v_h = 0.07c$ reported by Giroletti & Polatidis (2009; see also Angioni et al. 2019 for a more recent measurement). We note that our model assumes a source with perfectly symmetric morphology. Therefore, the model describes the evolution of one of the two lobes only, with the core-hotspot distance taken as $LS' = LS/2$, and the separation velocity of the hotspot from the core taken as $v'_h = v_h/2$. The luminosity of the modeled lobe is then multiplied by a factor of two to be compared with the observed lobes’ luminosity.

We fix the radio turnover frequency at the average of the values derived by Tingay et al. (2015) from ATCA observations of the source. We normalize the infrared blackbody component using the *Spitzer* flux at $16 \mu\text{m}$ (corresponding to frequency ν_{IR}). Given the dominance of starlight at optical frequencies in PKS 1718–649 and related uncertainties in the galaxy-AGN decomposition performed by Filippenko et al. (1985), for simplicity we fix the V-band and UV luminosities at ν_{star} and ν_{UV} (L_{star} , L_{UV} ; see Table 1) at values that result in both blackbody components having comparable fluxes at 3200 \AA , corresponding to $m_{\text{AB}} \sim 18$, where $m_{\text{AB}} = -2.5 \log(f_\nu) - 48.60$, and f_ν is in $\text{erg s}^{-1} \text{ cm}^{-2} \text{ Hz}$. We note that the blackbody component describing the visible light in our model matches rather well the W1 and W2 WISE measurements of Cutri et al. (2013).

The model assumes that the lobe electrons are in rough equipartition with the magnetic field and protons, and provide the bulk of the lobe pressure (e.g. Orienti & Dallacasa 2008, and references therein). The magnetic field is given by $B = (8\pi\eta_B p)^{1/2}$, with $\eta_B = U_B/p < 3$, where U_B denotes the magnetic field density. The electron energy density is $U_e = \eta_E p$ with $\eta_E \lesssim 3$. In this paper, we follow Stawarz et al. (2008) and we choose $\eta_E = 3$ and $\eta_B = 0.3$, which implies that the ratio of the model magnetic field density to the equipartition magnetic field density $U_B/U_B^{\text{eq}} = 0.1$, or $B/B^{\text{eq}} \sim 0.3$. We discuss this

assumption in Section 5.3 and show supplementary models with $\eta_B = 1$ and $\eta_B = 3$ in the Appendix.

As discussed in Stawarz et al. (2008), the likely shapes of the initial electron distribution injected into the radio lobes include a power-law function, $Q(\gamma) \propto \gamma^{-s}$, or a broken power-law function with the slope of the distribution changing from s_1 to s_2 at a given Lorentz factor γ_b . We test both possibilities. We choose $\gamma_{\min} = 1$ and $\gamma_{\max} = 100 m_p/m_e$.

We note that while Tingay et al. (2015) demonstrated that a proper description of the low-energy radio SED should include inhomogenous free-free absorption processes, we use the standard synchrotron self-absorbed spectrum. This choice does not affect the final high-energy shape of the γ -ray model SED because this regime is dominated by the IC scattering off high-energy electrons.

Given the above assumptions and observational constraints, we are left with only a handful of free model parameters: (i) the density of the ambient medium in which the lobes expand, n_0 ; (ii) the jet kinetic power, L_j ; (iii) the parameters of the electron energy distribution $Q(\gamma)$: the slope s if $Q(\gamma)$ is described by a single power function, or the slopes s_1 and s_2 of the lower- and higher-energy parts and the Lorentz factor corresponding to the break, γ_b , if $Q(\gamma)$ is described by a broken power-law function.

4. RESULTS

The expanding radio lobe model can successfully reproduce the bulk of the high-energy emission of PKS 1718–649. The IC scattering of the UV photons (presumably from an inner accretion flow) can account for the *Fermi*/LAT observational constraints, while the IC scattering of the infrared photons detected from the direction of PKS 1718–649, presumably due to the emission of a dusty environment in the galactic center, contributes to the source’s X-ray emission. We found that the contributions to the high energy emission of PKS 1718–649 coming from the IC scattering of the optical (galaxy) and synchrotron photons are negligible. The parameters of our final model are collected in Table 1 and the model SED is plotted in Figure 1. Below we describe our modeling rationale and results in detail.

Models with $Q(\gamma)$ in the form of a single power-law function were found to substantially overestimate the γ -ray emission and they failed to reproduce the observed γ -ray photon index. Thus, we concluded that the *Fermi*/LAT constraints require that the energy distribution of the electrons injected into the lobes of this source has a broken power-law form.

Beuchert et al. (2018) measured the intrinsic equivalent hydrogen absorbing column density from the direction of PKS 1718–649 and found that it varies in the $N_H \sim (3 - 7) \times 10^{21} \text{ cm}^{-2}$ range. The radii of the regions used in that work to extract the *Chandra* ($14''$) and *XMM-Newton* ($40''$) energy spectra correspond to ~ 4 and ~ 12 kpc, respectively, at the redshift of the source. Thus, the location of the intrinsic matter obscuring the nuclear X-rays cannot be determined on a parsec scale in PKS 1718–649 based on the modeling of Beuchert et al. (2018). We checked that with an extraction region size of $1.5''$ (~ 440 pc at the redshift of the source), approaching the spatial resolution of *Chandra*, the *Chandra* data of

TABLE 1
PARAMETERS OF THE BROADBAND SED MODEL

Description	Symbol	Model	Unit	Refs. ^a
Geometry of the radio source				
Linear size	LS	2	pc	(1) ^b
Hotspot sep. velocity	v_h	0.07	c	(1) ^b
Injected electron population $Q(\gamma)$				
Low-energy slope	s_1	1.9		(*) ^c
High-energy slope	s_2	3.2		(*)
Lorentz factor (min)	γ_{\min}	1		(3)
Lorentz factor (break)	γ_b	3	m_p/m_e	(*)
Lorentz factor (max)	γ_{\max}	100	m_p/m_e	(4)
Luminosities and characteristic frequencies				
Radio turnover freq.	ν_{peak}	3.25	GHz	(2) ^d
Jet kinetic power	L_j	2.2	$10^{42} \text{ erg s}^{-1}$	(*)
IR band ref. freq.	ν_{IR}	1.87	10^{13} Hz	...
νL_ν @ ν_{IR}	L_{IR}	8.05	$10^{42} \text{ erg s}^{-1}$	(5)
Visible band ref. freq.	ν_{star}	2.0	10^{14} Hz	...
νL_ν @ ν_{star}	L_{star}	1.1	$10^{44} \text{ erg s}^{-1}$	(6)
UV band ref. freq.	ν_{UV}	2.45	10^{15} Hz	...
νL_ν @ ν_{UV}	L_{UV}	8.5	$10^{42} \text{ erg s}^{-1}$	(6)
Environment				
ISM density	n_0	20	cm^{-3}	(*)
Electrons	η_E	3		(3) ^e
Magnetic field	η_B	0.3		(3, *) ^e
Additional power law X-ray emission				
Photon index	Γ	2.0		(*)
Luminosity (2–10 keV)	$L_{2-10 \text{ keV}}$	6.6	$10^{40} \text{ erg s}^{-1}$	(*)

Notes:

^a References: (*) This work; (1) Giroletti & Polatidis (2009); (2) Tingay et al. (2015); (3) Stawarz et al. (2008); (4) Ostorero et al. (2010); (5) Willett et al. (2010); (6) Filippenko (1985). ^b We use $LS' \simeq LS/2 = 1 \text{ pc}$ and $v_h' \simeq v_h/2 = 0.035c$ for core-hotspot linear size and separation velocity (c.f. Ostorero et al. 2010). ^c The radio spectral slope $\alpha \simeq 0.7$ (Tingay et al. 2015) suggests $s_1 = 2\alpha + 1 \simeq 2.4$ for the *evolved* electron distribution. ^d The average of the ν_{peak} values reported in Tingay et al. (2015). ^e Electron and magnetic field energy densities are parametrized as $U_E = \eta_E p$ and $U_B = \eta_B p$, where p stands for the expanding cocoon’s internal pressure.

the source (ObsIDs 16070 and 16623) are still consistent with intrinsic $N_H \sim (2-3) \times 10^{21} \text{ cm}^{-2}$. An intrinsic column density of the order of $3 \times 10^{21} \text{ cm}^{-2}$ implies a particle density within 440 kpc of $n_0 \sim 2.4 \text{ cm}^{-3}$. However, we found that models with n_0 of this order underestimate the ALMA and WMAP measurements (see Model A1 in Appendix; Figure 2 and Table 2). In particular, the continuum flux at 290 GHz measured by Maccagni et al. (2018) is underestimated by $\gtrsim 30\%$. A density an order of magnitude higher, $n_0 = 20 \text{ cm}^{-2}$, is required in order to fully account for the observed radio-to-submillimeter SED of PKS 1718–649 and this is the value we used in our broadband model. It implies that the X-ray N_H measured by Beuchert et al. (2018) is distributed uniformly within the central 50–100 pc.

The γ -ray spectrum (both the photon index and normalization) of PKS 1718–649 can be accounted for satisfactorily by a model with $s_1 = 1.9$, $s_2 = 3.2$, $\gamma_b = 3 m_p/m_e$, and jet kinetic power $L_j = 2.2 \times 10^{42} \text{ erg s}^{-1}$ (with the remaining model parameters fixed at the values derived from observations or assumed as described in Section 3). For these parameters, the model provided a good match also with observations in the radio and submillimeter bands. However, it returned an X-ray photon index that was much harder than the observed one, and it underestimated the observed soft X-ray emis-

sion. Given that PKS 1718–649 contains a LINER type AGN, it is possible that low luminosity nuclear emission contributes to the X-ray emission of the source. We modeled this with a cutoff power law function with $\Gamma = 2.0$, $E_{\text{cutoff}} = 100 \text{ keV}$, and 2–10 keV luminosity of $6.6 \times 10^{40} \text{ erg s}^{-1}$. We found that a sum of such a power-law component and IC scattering of the infrared photons in the radio lobes is able to fully explain the observed X-ray emission of PKS 1718–649.

5. DISCUSSION

We explored the applicability of the expanding radio lobe model (Stawarz et al. 2008) to the broadband radio-to- γ -ray SED of one of the youngest, most compact, and nearest symmetric radio source known to date, PKS 1718–649. Our modeling allowed us to uncover possible mechanisms responsible for the high-energy emission of the source and constrain interesting physical parameters of the source, such as the spectrum of the electrons injected from the hot spots into the lobes, and the jet kinetic power.

5.1. Origin of the γ -ray emission

We found that the properties of the γ -ray emission observed from PKS 1718–649 put strong constraints on the electron distribution $Q(\gamma)$ injected into the radio lobes. It is required that this distribution has a broken power-law shape characterized by a break energy $\gamma_b = 3 m_p/m_e$ and a high-energy slope $s_2 = 3.2$. The radio and submillimeter data imply that the lower-energy segment ($\gamma < \gamma_b$) of $Q(\gamma)$ has index $s_1 = 1.9$ and the lobes expand in a relatively dense medium with $n_0 = 20 \text{ cm}^{-3}$.

The electron population of the radio lobes evolves during the lobes’ expansion due to the adiabatic and radiative cooling effects (Stawarz et al. 2008). In the case of a broken power-law injection, the electron spectral continuum steepens at $\gamma > \gamma_{\text{cr}} = 200 \eta_B^{-1} L_{j,45}^{-1/2}$ when compared to the injected one, where $L_{j,45} \equiv L_j/10^{45} \text{ erg s}^{-1}$. In our model solution for PKS 1718–649, γ_{cr} corresponds to $\sim 7.7 m_p/m_e$ or $\sim 2.6 \gamma_b$. The s_1 index is close to the canonical spectrum generated by diffusive (first-order Fermi) shock acceleration and comparable with the low-energy slopes derived by Ostorero et al. (2010) for a sample of eleven GPS/CSO galaxies known as X-ray emitters up to 2008. The density n_0 is of the same order as the mean density found by Mukherjee et al. (2016; 2017) who fitted the probability density function of the simulated density of an ISM evolving in the presence of an expanding jet with jet head $\lesssim 1 \text{ kpc}$ using a modified lognormal function proposed by Hopkins (2013; see also Zovaro et al. 2019).

5.2. Origin of the X-ray emission

We showed that, while the γ -ray emission in PKS 1718–649 is consistent with IC scattering of the UV photons from an accretion flow off energetic electrons in the radio lobes, the origin of the X-ray emission is more elusive. Beuchert et al. (2018) modeled the primary X-ray emission with a single power-law function and associated it with an X-ray corona. We showed that the IC scattering of the infrared ambient photons, likely due to the emission of the dusty environment of PKS 1718–649 resolved with VLT and ALMA (Maccagni

et al. 2016; 2018), contributes to the X-ray emission of the source. However, its photon index is harder than that derived from the observations. As a result, the model was found to underestimate the soft X-ray emission of the source. We proposed that an additional component is required in order to fully explain the observed intrinsic X-ray emission, and we modeled it with a power-law function with a photon index $\Gamma = 2.0$, a 2-10 keV luminosity $L_{2-10\text{ keV}} = 6.6 \times 10^{40} \text{ erg s}^{-1}$ and a high-energy cutoff at 100 keV (even though the current data cannot confirm or reject the presence of such a cutoff). Interestingly, these parameters are typical for LINER type AGNs studied in X-rays (e.g. Gonzalez-Martin et al. 2009). This additional component may be associated with a weak X-ray corona or a radiatively inefficient nuclear emission (e.g. an ADAF; Ichimaru 1977; Narayan & Yi 1994; 1995a; 1995b; Abramowicz et al. 1995; Chen et al. 1995). The sum of the IC X-ray emission from the radio lobes and low luminosity nucleus agrees with the X-ray constraints derived by Beuchert et al. (2018) using a single power-law function, within the error bars (see Figure 1).

However, we stress that the relative contributions of a low luminosity nucleus and IC scattering of the infrared photons in the radio lobes are difficult to constrain with the current data. It is possible that only a fraction of the IR emission measured with *Spitzer* intersects the expanding radio lobes, given the small size of the radio source in PKS 1718–649 ($LS = 2 \text{ pc}$) and the complex structures in the innermost 15 kpc of the host galaxy of PKS 1718–649. Indeed, resolved measurements with ALMA revealed a CO gas distributed in a complex warped disk, forming a circumnuclear disk at $r \lesssim 700 \text{ pc}$, and molecular clouds falling onto the central supermassive black hole at $r \lesssim 75 \text{ pc}$ (Maccagni et al. 2018). We estimated that if only half of the infrared emission becomes IC scattered in the radio lobes, then our modeling requires a nuclear power-law X-ray component with $L_{2-10\text{ keV}} = 5.5 \times 10^{40} \text{ erg s}^{-1}$, which is still well within the range of the 2-10 keV luminosities reported in the literature for the LINER-type galaxies.

We note that our model predicts a spectral hardening above 10 keV where the IC component from the radio lobes dominates over the nuclear emission. This could be tested with observations in the hard X-ray band. In addition, the high energy SED of PKS 1718–649 peaks in the MeV range, making PKS 1718–649 an ideal target for future MeV-band missions such as AMEGO.

5.3. Jet kinetic power and feedback

The jet kinetic power resulting from our modeling, $L_j = 2.2 \times 10^{42} \text{ erg s}^{-1}$ is in excellent agreement with the upper limit reported by Maccagni et al. (2014; $L_j < 2 \times 10^{43} \text{ erg s}^{-1}$). This jet power is lower than the values found for powerful flat-spectrum radio quasars (FSRQs) and BL Lacertae sources (e.g., Sambruna et al. 2006; Ghisellini et al. 2009), as well as for FRI/FRII radio galaxies (e.g., Laing et al. 2002; Croston et al. 2008, 2009; Croston et al. 2018 and references therein; see also Xu et al. 2009).

The implied magnetic field intensity within the lobes is $\sim 4.3 \text{ mG}$, in agreement with expectations for compact young lobes. The assumed value of $\eta_B = 0.3$ suggests a moderate departure of the magnetic field strength,

within one order of magnitude, from equipartition, which is supported by observations (e.g. Ineson et al. 2017, Croston et al. 2018; see, however, Orienti & Dallacasa 2008). In the Appendix (Figure 2), we present models with $\eta_B = 1$ (Model A2) and $\eta_B = 3$ (Model A3; equipartition) in order to demonstrate that models with higher η_B have difficulties in accounting for the high-energy emission in PKS 1718–649: the X-ray band becomes dominated by an additional X-ray component in these models, and the soft γ -ray emission is underestimated (given the *Fermi*/LAT 1σ confidence level model constraints by Principe et al. 2021). We stress that the jet powers resulting from our preferred model (Figure 1, Table 1) and from models A2-A3 vary at most by a factor of ~ 3 (Table 2), indicating that our estimate of L_j is robust.

Mukherjee et al. (2016; 2017) showed with numerical simulations that the feedback of low-power jets is significant because they are confined by the ISM for a longer time than their more powerful counterparts. This affects the ISM density distribution and inhibits the star formation. Indeed, Willett et al. (2010) reported a rather weak star formation rate in PKS 1718–649, $0.8\text{--}1.9 M_\odot \text{ yr}^{-1}$, estimated by means of PAH signatures measured with *Spitzer*. Interestingly, Mukherjee et al. (2017) argued that jets with power $\lesssim 10^{43} \text{ erg s}^{-1}$, such as those of PKS 1718–649, may be too weak to escape the ISM confinement, and too weakly pressurized to prevent an infall of gas back into the initially created central cavity.

5.4. Mass accretion rate and gas mass reservoir

We use the relation of Allen et al. (2006) to translate L_j into the Bondi accretion power, $L_{\text{bondi}} = 2.2 \times 10^{43} \text{ erg s}^{-1}$. Assuming an accretion efficiency $\epsilon = 0.1$, the Bondi accretion rate is $\dot{M} = 0.004 M_\odot/\text{yr}$. If the intrinsic N_{H} measured in the X-ray band (Beuchert et al. 2018) is indeed distributed uniformly over a surface area with a radius $r = 50\text{--}100 \text{ pc}$, as suggested by the submillimeter band which favors a relatively high ambient density of $n_0 = 20 \text{ cm}^{-3}$, then the gas mass reservoir within this radius is of the order of $(0.3\text{--}1.3) \times 10^6 M_\odot$, providing an ample supply to feed the central black hole. Both the mass accretion rate and the gas mass reservoir we find in this work are compatible with those reported by Maccagni et al. (2018), who inferred the presence of cold clouds falling onto the central black hole within $\lesssim 75 \text{ pc}$ by studying tracers such as H_1 , H_2 and ^{12}CO (2–1) with ALMA and SINFONI (Maccagni et al. 2016; 2018). They found an accretion rate $1.3 \times 10^{-3} M_\odot \text{ yr}^{-1} \lesssim \dot{M}_{\text{H}_2} \lesssim 2.2 M_\odot \text{ yr}^{-1}$, and a mass of the absorbing molecular clouds in the $3 \times 10^2 M_\odot - 5 \times 10^5 M_\odot$ range.

The mass accretion rate that we found, expressed in terms of the Eddington accretion rate, is $\dot{M} = 5 \times 10^{-4} \dot{M}_{\text{Edd}}$, assuming the mean of the two black hole mass estimates in Willett et al. (2010). On the other hand, the UV luminosity in our model, $L_{\text{UV}} \simeq 8.5 \times 10^{42} \text{ erg s}^{-1}$, implies an accretion rate of the order of $\dot{M} \simeq 2 \times 10^{-4} \dot{M}_{\text{Edd}}$. Both estimates are consistent with the LINER classification of the active nucleus in PKS 1718–649.

5.5. Transverse expansion

The transverse size and recent-day transverse expansion velocity resulting from our modeling are $l_c = 2.6$ pc and $v_c = 0.13c$, respectively. They are larger than their counterpart parameters along the core-hotspot direction (i.e., the core-hotspot distance, LS' , and the core-hotspot separation velocity, v'_h). Thus, the model suggests that the lobes of PKS 1718–649, and other extremely compact radio sources, may be more elongated in the transverse direction than in the direction of the hotspots. Some evidence for this can be seen at least for the northern lobe on the 8.4 GHz VLBI radio maps recently presented by Angioni et al. (2019). Since $l_c \propto LS'^{1/2}$ and $v_c \propto LS'^{-1/2}$, the model predicts that eventually the transverse expansion will slow down; in PKS 1718–649, v_c will be comparable to v'_h once LS' reaches ~ 15 pc, and the source will evolve to a state in which $l_c < LS'$.

6. CONCLUSIONS

We demonstrated that the expanding radio lobe model by Stawarz et al. (2008) can explain the high-energy emission in PKS 1718–649, the first and one of only a few young radio sources detected to date in the γ -ray band with *Fermi*/LAT, as being due to IC scattering of the IR and UV emission off energetic electrons injected into the lobes from the hotspots, assuming a rough equipartition between the magnetic field and particles, and an additional contribution from a weak X-ray corona or an ADAF at the luminosity level expected in LINER type AGNs. Our results suggest that PKS 1718–649 is destined to evolve into a low-power FRI type radio galaxy. Low power jets, like those in PKS 1718–649, are important for the jet/galaxy feedback process because they struggle to propagate through the ISM on their way out from the host galaxy, and interact with the gas in the host galaxies for a longer time than their more powerful counterparts.

Based on our modeling of PKS 1718–649, we were able to estimate the magnetic field intensity within the lobes,

the shape of the distribution of the evolved electrons in the lobes, the properties of the transverse lobe expansion, the mass accretion rate, and the gas mass reservoir available to feed the black hole.

The expanding radio lobe model has recently been considered by Lister et al. (2020) in a discussion of the high-energy SED of another γ -ray detected CSO, TXS 0128+554. The authors reported that the observed *Fermi*/LAT flux of TXS 0128+554 is three orders of magnitude higher than predicted γ -ray emission from the lobes, and concluded that it most likely originates in the inner jet/core region rather than in the lobes. Furthermore, Sobolewska et al. (2019b) concluded that the expanding radio lobe model for a set of model parameters considered by Ostorero et al. (2010) for OQ+208, a CSO embedded in a cloud of matter with an intrinsic absorbing column density of the order of 10^{24} cm $^{-2}$ (however, with no γ -ray detection to date), appears to overestimate the level of the X-ray emission measured from a joint modeling of *Chandra*, *XMM-Newton* and *NuSTAR* data. Thus, it remains to be determined if the model of expanding radio lobes provides a universal explanation of the X-ray and γ -ray emission of the Compact Symmetric Objects and other GPS galaxies, or if they form a heterogeneous population with respect to the origin of their high-energy emission.

MS and AS were supported by NASA contract NAS8-03060 (Chandra X-ray Center). MS acknowledges partial support by the NASA contracts 80NSSC18K1609 and 80NSSC19K1311. Partial support for this work was provided by the NASA grants GO1-12145X, GO4-15099X. LO acknowledges partial support from the INFN grant InDark and the Italian Ministry of Education, University and Research (MIUR) under the Departments of Excellence grant L.232/2016. This research has made use of NASA's Astrophysics Data System Bibliographic Services. The authors thank Rafał Moderski for making his numerical code of expanding radio lobes available for this study.

APPENDIX

MODEL SOLUTIONS WITH LOWER AMBIENT DENSITY AND HIGHER η_B

REFERENCES

- Abdollahi, S., Acero, F., Ackermann, M., et al. 2020, *ApJS*, 247, 33. doi:10.3847/1538-4365/ab6bcb
- Abramowicz, M. A., Chen, X., Kato, S., et al. 1995, *ApJ*, 438, L37. doi:10.1086/187709
- Astropy Collaboration, Robitaille, T. P., Tollerud, E. J., et al. 2013, *A&A*, 558, A33. doi:10.1051/0004-6361/201322068
- Astropy Collaboration, Price-Whelan, A. M., Sipőcz, B. M., et al. 2018, *AJ*, 156, 123. doi:10.3847/1538-3881/aabc4f
- An, T. & Baan, W. A. 2012, *ApJ*, 760, 77. doi:10.1088/0004-637X/760/1/77
- Angioni, R., Ros, E., Kadler, M., et al. 2019, *A&A*, 627, A148. doi:10.1051/0004-6361/201935697
- Begelman, M. C. & Cioffi, D. F. 1989, *ApJ*, 345, L21. doi:10.1086/185542
- Bennett, C. L., Hill, R. S., Hinshaw, G., et al. 2003, *ApJS*, 148, 97. doi:10.1086/377252
- Bentz, M. C., Peterson, B. M., Pogge, R. W., et al. 2009, *ApJ*, 694, L166. doi:10.1088/0004-637X/694/2/L166
- Beuchert, T., Rodríguez-Ardila, A., Moss, V. A., et al. 2018, *A&A*, 612, L4. doi:10.1051/0004-6361/201833064
- Bicknell, G. V., Dopita, M. A., & O'Dea, C. P. O. 1997, *ApJ*, 485, 112. doi:10.1086/304400
- Bolton, J. G. & Butler, P. W. 1975, *Australian Journal of Physics Astrophysical Supplement*, 34, 33
- Chen, X., Abramowicz, M. A., Lasota, J.-P., et al. 1995, *ApJ*, 443, L61. doi:10.1086/187836
- Chen, X. & Wright, E. L. 2009, *ApJ*, 694, 222. doi:10.1088/0004-637X/694/1/222
- Croston, J. H., Hardcastle, M. J., Birkinshaw, M., et al. 2008, *MNRAS*, 386, 1709. doi:10.1111/j.1365-2966.2008.13162.x
- Croston, J. H., Kraft, R. P., Hardcastle, M. J., et al. 2009, *MNRAS*, 395, 1999. doi:10.1111/j.1365-2966.2009.14715.x
- Croston, J. H., Ineson, J., & Hardcastle, M. J. 2018, *MNRAS*, 476, 1614. doi:10.1093/mnras/sty274
- Cutri, R. M., Wright, E. L., Conrow, T., et al. 2013, *Explanatory Supplement to the ALLWISE Data Release Products*, by R. M. Cutri et al.
- Dasyra, K. M., Ho, L. C., Armus, L., et al. 2008, *ApJ*, 674, L9. doi:10.1086/528843

TABLE 2
PARAMETERS OF THE SED MODEL WITH LOW AMBIENT DENSITY.

Description	Symbol	Model A1	Model A2	Model A3	Unit	Refs. ^a
Geometry of the radio source						
Linear size	LS	2	2	2	pc	(1) ^b
Hotspot sep. velocity	v_h	0.07	0.07	0.07	c	(1) ^b
Injected electron population $Q(\gamma)$						
Low-energy slope	s_1	2.1	1.9	1.9		(*) ^c
High-energy slope	s_2	3.3	3.2	3.1		(*)
Lorentz factor (min)	γ_{\min}	1	1	1		(3)
Lorentz factor (break)	γ_b	3	6	12	m_p/m_e	(*)
Lorentz factor (max)	γ_{\max}	100	100	100	m_p/m_e	(4)
Luminosities and characteristic frequencies						
Radio turnover freq.	ν_{peak}	3.25	3.25	3.25	GHz	(2) ^d
Jet kinetic power	L_j	5.5	1.2	0.7	$10^{42} \text{ erg s}^{-1}$	(*)
IR band ref. freq.	ν_{IR}	1.87	1.87	1.87	10^{13} Hz	...
$\nu L_\nu @ \nu_{\text{IR}}$	L_{IR}	8.05	8.05	8.05	$10^{42} \text{ erg s}^{-1}$	(5)
Visible band ref. freq.	ν_{star}	2.0	2.0	2.0	10^{14} Hz	...
$\nu L_\nu @ \nu_{\text{star}}$	L_{star}	1.1	1.1	1.1	$10^{44} \text{ erg s}^{-1}$	(6)
UV band ref. freq.	ν_{UV}	2.45	2.45	2.45	10^{15} Hz	...
$\nu L_\nu @ \nu_{\text{UV}}$	L_{UV}	8.5	8.5	8.5	$10^{42} \text{ erg s}^{-1}$	(6)
Environment						
ISM density	n_0	3	20	20	cm^{-3}	(*)
Electrons	η_E	3	3	3		(3) ^e
Magnetic field	η_B	0.3	1	3		(3, *) ^e
Additional power law X-ray emission						
Photon index	Γ	not required	1.9	1.8		(*)
Luminosity (2-10 keV)	$L_{2-10 \text{ keV}}$	n/a	1.3	1.7	$10^{41} \text{ erg s}^{-1}$	(*)

Notes:

^a The star symbols (*) mark model parameters derived in this work. Other references: (1) Giroletti & Polatidis (2009), (2) Tingay et al. (2015), (3) Stawarz et al. (2008), (4) Ostorero et al. (2010), (5) Willett et al. (2010), (6) Filippenko (1985). ^b We use $LS' \simeq LS/2 = 1 \text{ pc}$ and $v_h' \simeq v_h/2 = 0.035c$ for core-hotspot linear size and separation velocity (c.f. Ostorero et al. 2010). ^c The radio spectral slope $\alpha \simeq 0.7$ (Tingay et al. 2015) suggests $s_1 = 2\alpha + 1 \simeq 2.4$ for the *evolved* electron distribution. ^d The average of the ν_{peak} values reported in Tingay et al. (2015). ^e Electron and magnetic field energy densities are parametrized as $U_E = \eta_E p$ and $U_B = \eta_B p$, where p stands for the expanding cocoon's internal pressure.

Fanaroff, B. L. & Riley, J. M. 1974, MNRAS, 167, 31P.
doi:10.1093/mnras/167.1.31P

Filippenko, A. V. 1985, ApJ, 289, 475. doi:10.1086/162909

Ghisellini, G., Tavecchio, F., & Ghirlanda, G. 2009, MNRAS, 399, 2041. doi:10.1111/j.1365-2966.2009.15397.x

Giommi, P., Colafrancesco, S., Padovani, P., et al. 2009, A&A, 508, 107. doi:10.1051/0004-6361/20078905

Gold, B., Odegard, N., Weiland, J. L., et al. 2011, ApJS, 192, 15. doi:10.1088/0067-0049/192/2/15

González-Martín, O., Masegosa, J., Márquez, I., et al. 2009, A&A, 506, 1107. doi:10.1051/0004-6361/200912288

Gregory, P. C., Vavasour, J. D., Scott, W. K., et al. 1994, ApJS, 90, 173. doi:10.1086/191862

Healey, S. E., Romani, R. W., Taylor, G. B., et al. 2007, ApJS, 171, 61. doi:10.1086/513742

Hinshaw, G., Larson, D., Komatsu, E., et al. 2013, ApJS, 208, 19. doi:10.1088/0067-0049/208/2/19

Hopkins, P. F. 2013, MNRAS, 430, 1880. doi:10.1093/mnras/stt010

Ichimaru, S. 1977, ApJ, 214, 840. doi:10.1086/155314

Ineson, J., Croston, J. H., Hardcastle, M. J., et al. 2017, MNRAS, 467, 1586. doi:10.1093/mnras/stx189

Kawakatu, N. & Kino, M. 2006, MNRAS, 370, 1513. doi:10.1111/j.1365-2966.2006.10574.x

Laing, R. A. & Bridle, A. H. 2002, MNRAS, 336, 1161. doi:10.1046/j.1365-8711.2002.05873.x

Lister, M. L., Homan, D. C., Kovalev, Y. Y., et al. 2020, ApJ, 899, 141. doi:10.3847/1538-4357/aba18d

Maccagni, F. M., Morganti, R., Oosterloo, T. A., et al. 2014, A&A, 571, A67. doi:10.1051/0004-6361/201424334

Maccagni, F. M., Santoro, F., Morganti, R., et al. 2016, A&A, 588, A46. doi:10.1051/0004-6361/201528016

Maccagni, F. M., Morganti, R., Oosterloo, T. A., et al. 2018, A&A, 614, A42. doi:10.1051/0004-6361/201732269

Massardi, M., Ekers, R. D., Murphy, T., et al. 2008, MNRAS, 384, 775. doi:10.1111/j.1365-2966.2007.12751.x

Massardi, M., López-Caniego, M., González-Nuevo, J., et al.

2009, MNRAS, 392, 733. doi:10.1111/j.1365-2966.2008.14084.x

Mauch, T., Murphy, T., Buttery, H. J., et al. 2003, MNRAS, 342, 1117. doi:10.1046/j.1365-8711.2003.06605.x

Meyer, M. J., Zwaan, M. A., Webster, R. L., et al. 2004, MNRAS, 350, 1195. doi:10.1111/j.1365-2966.2004.07710.x

Migliori, G., Siemiginowska, A., Sobolewska, M., et al. 2016, ApJ, 821, L31. doi:10.3847/2041-8205/821/2/L31

Mukherjee, D., Bicknell, G. V., Sutherland, R., et al. 2016, MNRAS, 461, 967. doi:10.1093/mnras/stw1368

Mukherjee, D., Bicknell, G. V., Sutherland, R., et al. 2017, MNRAS, 471, 2790. doi:10.1093/mnras/stx1749

Müller, C., Burd, P. R., Schulz, R., et al. 2016, A&A, 593, L19. doi:10.1051/0004-6361/201629547

Murphy, T., Sadler, E. M., Ekers, R. D., et al. 2010, MNRAS, 402, 2403. doi:10.1111/j.1365-2966.2009.15961.x

Narayan, R. & Yi, I. 1994, ApJ, 428, L13. doi:10.1086/187381

Narayan, R. & Yi, I. 1995, ApJ, 444, 231. doi:10.1086/175599

Narayan, R. & Yi, I. 1995, ApJ, 452, 710. doi:10.1086/176343

O'Dea, C. P. 1998, PASP, 110, 493. doi:10.1086/316162

O'Dea, C. P. & Siemiginowska, A. 2016, Astronomische

Nachrichten, 337, 205. doi:10.1002/asna.201512281

O'Dea, C. P. & Saikia, D. J. 2021, A&A Rev., 29, 3. doi:10.1007/s00159-021-00131-w

Ojha, R., Kadler, M., Böck, M., et al. 2010, A&A, 519, A45. doi:10.1051/0004-6361/200912724

Orienti, M., 2016, AN, 337, 9. doi:10.1002/asna.201512257

Orienti, M. & Dallacasa, D. 2008, A&A, 487, 885. doi:10.1051/0004-6361:200809948

Ostorero, L., Moderski, R., Stawarz, L., et al. 2010, ApJ, 715, 1071. doi:10.1088/0004-637X/715/2/1071

Polatidis, A. G. & Conway, J. E. 2003, PASA, 20, 69. doi:10.1071/AS02053

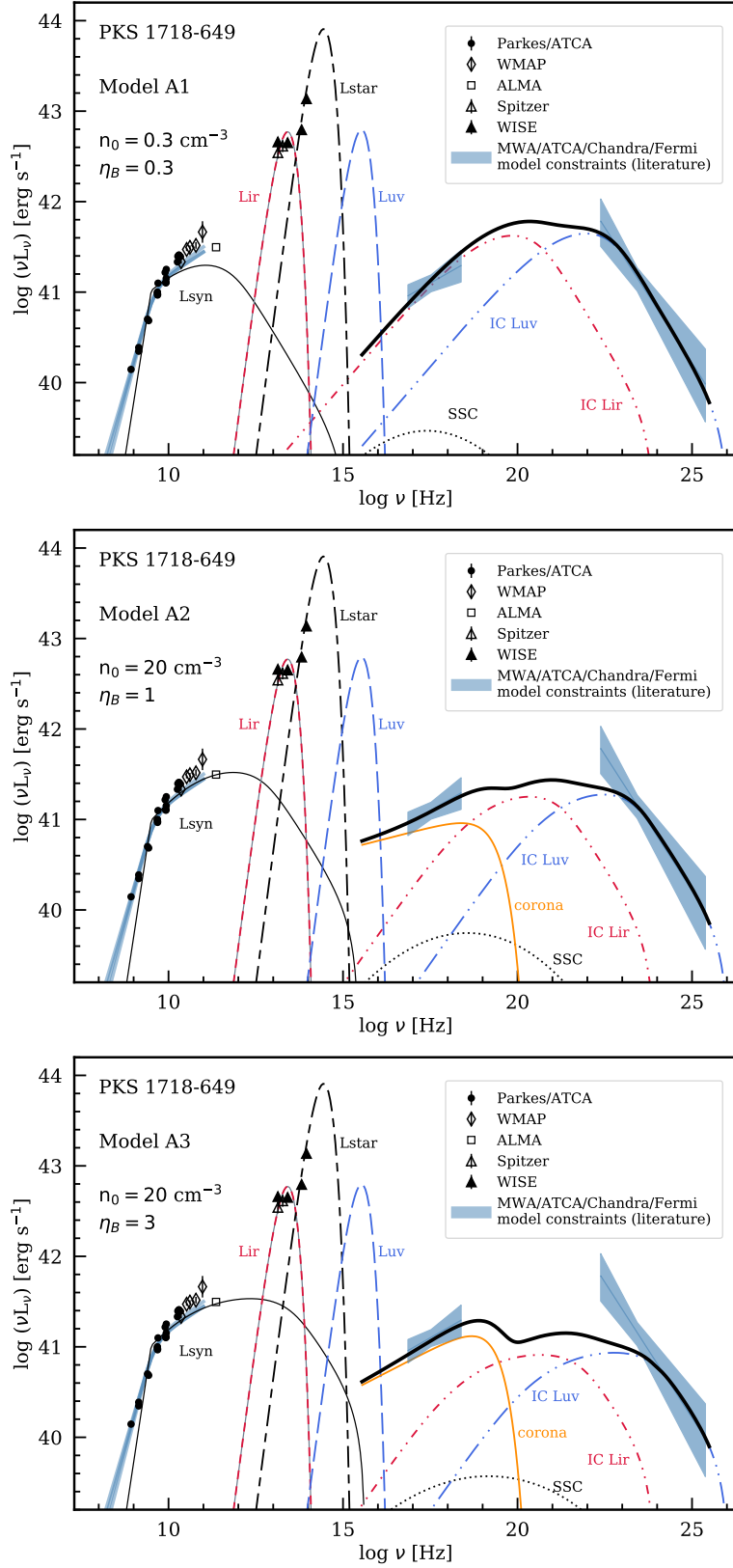


FIG. 2.— The same as Figure 1 but for Model A1 with a low ambient density of $n_0 = 3 \text{ cm}^{-3}$; Model A2 with $\eta_B = 1$; and Model A3 with $\eta_B = 3$ (equipartition). See Table 2 for model parameters. It can be seen that models with ambient density of the order of $n_0 \sim 3 \text{ cm}^{-3}$ underestimate the WMAP and ALMA measurements (see Section 4). Models with $\eta_B \sim 1$ –3 underestimate the soft γ -ray flux and require that an additional component accounts for the bulk of the X-ray flux (see Section 5.3).

- Principe, G., Migliori, G., Johnson, T. J., et al. 2020, *A&A*, 635, A185. doi:10.1051/0004-6361/201937049
- Principe, G., Di Venere, L., Orienti, M., et al. 2021, *MNRAS*, 507, 4564. doi:10.1093/mnras/stab2357
- Ricci, R., Prandoni, I., Gruppioni, C., et al. 2006, *A&A*, 445, 465. doi:10.1051/0004-6361:20053797
- Sadler, E. M., Ricci, R., Ekers, R. D., et al. 2006, *MNRAS*, 371, 898. doi:10.1111/j.1365-2966.2006.10729.x
- Sambruna, R. M., Gliozzi, M., Tavecchio, F., et al. 2006, *ApJ*, 652, 146. doi:10.1086/507420
- Siemiginowska, A. 2009, *Astronomische Nachrichten*, 330, 264. doi:10.1002/asna.200811172
- Siemiginowska, A., Sobolewska, M., Migliori, G., et al. 2016, *ApJ*, 823, 57. doi:10.3847/0004-637X/823/1/57
- Sobolewska, M., Siemiginowska, A., Guainazzi, M., et al. 2019a, *ApJ*, 871, 71. doi:10.3847/1538-4357/aace78
- Sobolewska, M., Siemiginowska, A., Guainazzi, M., et al. 2019b, *ApJ*, 884, 166. doi:10.3847/1538-4357/ab3ec3
- Stawarz, L., Ostorero, L., Begelman, M. C., et al. 2008, *ApJ*, 680, 911. doi:10.1086/587781
- Tingay, S. J., Jauncey, D. L., Reynolds, J. E., et al. 1997, *AJ*, 113, 2025. doi:10.1086/118414
- Tingay, S. J., Reynolds, J. E., Tzioumis, A. K., et al. 2002, *ApJS*, 141, 311. doi:10.1086/340783
- Tingay, S. J. & de Kool, M. 2003, *AJ*, 126, 723. doi:10.1086/376600
- Tingay, S. J., Macquart, J.-P., Collier, J. D., et al. 2015, *AJ*, 149, 74. doi:10.1088/0004-6256/149/2/74
- Veron-Cetty, M.-P., Woltjer, L., Ekers, R. D., et al. 1995, *A&A*, 297, L79
- Wilkinson, P. N., Polatidis, A. G., Readhead, A. C. S., et al. 1994, *ApJ*, 432, L87. doi:10.1086/187518
- Willett, K. W., Stocke, J. T., Darling, J., et al. 2010, *ApJ*, 713, 1393. doi:10.1088/0004-637X/713/2/1393
- Wright, A. E., Wark, R. M., Troup, E., et al. 1990, *PASA*, 8, 261
- Wright, E. L., Chen, X., Odegard, N., et al. 2009, *ApJS*, 180, 283. doi:10.1088/0067-0049/180/2/283
- Xu, Y.-D., Cao, X., & Wu, Q. 2009, *ApJ*, 694, L107. doi:10.1088/0004-637X/694/2/L107
- Zovaro, H. R. M., Sharp, R., Nesvadba, N. P. H., et al. 2019, *MNRAS*, 484, 3393. doi:10.1093/mnras/stz233